

J-PLUS: Support vector regression to measure stellar parameters

Cunshi Wang^{1,2}, Yu Bai¹, Haibo Yuan³, Jifeng Liu^{1,2}, J.A. Fernández-Ontiveros⁴, Paula R. T. Coelho⁵, F. Jiménez-Esteban⁶, Carlos Andrés Galarza⁷, R. E. Angulo^{8,9}, A. J. Cenarro⁴, D. Cristóbal-Hornillos⁴, R. A. Dupke^{7,10,11}, A. Ederoclite⁴, C. Hernández-Monteagudo^{12,13}, C. López-Sanjuan⁴, A. Marín-Franch⁴, M. Moles⁴, L. Sodr e Jr.⁵, H. Vázquez Rami o⁴, and J. Varela⁴

¹ Key Laboratory of Optical Astronomy, National Astronomical Observatories, Chinese Academy of Sciences, 20A Datun Road, Chaoyang District, Beijing 100012, People's Republic of China

² College of Astronomy and Space Sciences, University of Chinese Academy of Sciences, Beijing 100049, China

³ Department of Astronomy, Beijing Normal University, Beijing 100875, People's Republic of China

⁴ Centro de Estudios de F sica del Cosmos de Arag n (CEFCA), Unidad Asociada al CSIC, Plaza San Juan 1, 44001 Teruel, Spain

⁵ Instituto de Astronomia, Geof sica e Ci ncias Atmosf ricas, Universidade de S o Paulo, 05508-090 S o Paulo, Brazil

⁶ Departamento de Astrof sica, Centro de Astrobiolog a (CSIC-INTA), ESAC Campus, Camino Bajo del Castillo s/n, E-28692 Villanueva de la Ca ada, Madrid, Spain

⁷ Observat rio Nacional - MCTI (ON), Rua Gal. Jos  Cristino 77, S o Crist v o, 20921-400 Rio de Janeiro, Brazil

⁸ Donostia International Physics Centre (DIPC), Paseo Manuel de Lardizabal 4, 20018 Donostia-San Sebasti n, Spain

⁹ IKERBASQUE, Basque Foundation for Science, 48013, Bilbao, Spain

¹⁰ University of Michigan, Department of Astronomy, 1085 South University Ave., Ann Arbor, MI 48109, USA

¹¹ University of Alabama, Department of Physics and Astronomy, Gallalee Hall, Tuscaloosa, AL 35401, USA

¹² Instituto de Astrof sica de Canarias, La Laguna, 38205, Tenerife, Spain

¹³ Departamento de Astrof sica, Universidad de La Laguna, 38206, Tenerife, Spain

Received April 29, 2022; accepted April 29, 2022

ABSTRACT

Context. Stellar parameters are among the most important characteristics in studies of stars which, in traditional methods, are based on atmosphere models. However, time, cost, and brightness limits restrain the efficiency of spectral observations. The Javalambre Photometric Local Universe Survey (J-PLUS) is an observational campaign that aims to obtain photometry in 12 bands. Owing to its characteristics, J-PLUS data have become a valuable resource for studies of stars. Machine learning provides powerful tools for efficiently analyzing large data sets, such as the one from J-PLUS, and enables us to expand the research domain to stellar parameters. **Aims.** The main goal of this study is to construct a support vector regression (SVR) algorithm to estimate stellar parameters of the stars in the first data release of the J-PLUS observational campaign.

Methods. The training data for the parameters regressions are featured with 12-waveband photometry from J-PLUS and are cross-identified with spectrum-based catalogs. These catalogs are from the Large Sky Area Multi-Object Fiber Spectroscopic Telescope, the Apache Point Observatory Galactic Evolution Experiment, and the Sloan Extension for Galactic Understanding and Exploration. We then label them with the stellar effective temperature, the surface gravity, and the metallicity. Ten percent of the sample is held out to apply a blind test. We develop a new method, a multi-model approach, in order to fully take into account the uncertainties of both the magnitudes and the stellar parameters. The method utilizes more than two hundred models to apply the uncertainty analysis.

Results. We present a catalog of 2,493,424 stars with the root mean square error of 160K in the effective temperature regression, 0.35 in the surface gravity regression, and 0.25 in the metallicity regression. We also discuss the advantages of this multi-model approach and compare it to other machine-learning methods.

Key words. methods: data analysis – techniques: spectroscopic - astronomical databases: miscellaneous

1. Introduction

In modern astronomy, the large amount of raw data produced by the newest surveys is far beyond our traditional processing capacity, and this insufficient computing power has become a bottleneck to the rapid development of astrophysics. Fortunately, the development of computer science has provided us with new ways to understand and gain knowledge from these raw data. Machine learning in particular has achieved remarkable success in offering novel solutions to complex problems based on applications of loss functions, optimization methods (Ruder 2017), and statistical models (MacKay 2003). Owing to its nonfunctional algorithms (Cortes & Vapnik 1995; Boser et al. 1992; Cristianini & Shawe-Taylor 2000; Cover & Hart 1967; Stone 1977;

Quinlan 1986; Breiman 2001), machine learning can reveal potential patterns and important parameters that are indistinguishable using traditional scientific or statistical methods.

Stars are the cornerstone of astronomy, and stellar parameters are among the most crucial characteristics of understanding and characterizing stars. Among the most powerful and accurate methods of determining stellar parameters is spectral analysis (Wu et al. 2011; Boeche et al. 2018; Anguiano, B. et al. 2018).

However, spectral observations can be costly. The most powerful spectroscopy survey — the Large Sky Area Multi-Object Fiber Spectroscopy Telescope (LAMOST) — has taken spectra of about ten million stars in low resolution and about three million in medium resolution with a four-meter telescope in

the past 8 years. In contrast to spectral observations, photometric observations have much higher observational efficiency. Compared to LAMOST, the Javalambre Photometric Local Universe Survey (J-PLUS, Cenarro et al. 2019) observed 223.6 million objects in its five-year observational campaign¹. Therefore, many studies have been working on estimating stellar parameters from photometry-based data by constructing models of photometric observation results (Bailer-Jones 2011; Sichevskij 2012; Sichevskij et al. 2014). Their modeling requires highly precise photometric data from a few surveys, while another mighty tool — machine learning — can reveal the distribution or pattern hidden inside the photometry with rougher data.

Machine learning, a cross-disciplinary subject of statistics, optimization, and computer science, creates algorithms that can process data based on a well-chosen sample set with features. Different algorithms assign different models and reveal potential patterns in the sample (MacKay 2003; Shalev-Shwartz & Ben-David 2014). The algorithms select features from samples and optimize the parameters based on a given loss function. The loss function evaluates the difference between the predicted result and the true value. Machine-learning algorithms have been applied in many different disciplines, including finance, medical science, and computer vision.

Machine-learning technology has shown the ability to obtain valuable information from multi-band photometric data. Several studies have made some efforts to determine stellar parameters from photometric surveys. Bai et al. (2019) have derived stellar effective temperatures from *Gaia* second data release using a random forest (RF) algorithm. Bai et al. (2018) have presented RF models to categorize objects such as stars, galaxies, and quasi-stellar objects (QSOs) and classified and obtained the effective temperature of stars. Lu & Li (2015) developed a scheme to achieve stellar parameters from the Least Absolute Shrinkage and Selection Operator (LASSO) algorithm and support vector regression (SVR) models. Yang et al. (2021) designed a cost-sensitive artificial neural network and achieved stellar parameters from two million stars from the J-PLUS first data release (DR1). Galarza et al. (2022) developed the stellar parameters estimation based on the ensemble methods (SPEEM) pipeline, which is a stack of feature searching, normalization, and multi-output regressor. The SPEEM is based on RF and extreme gradient boosting (XGB). These works are all based on machine-learning algorithms which indicates their powerful ability to reveal potential patterns within data.

J-PLUS has also been used to gain knowledge of objects ranging from our Solar System to the deep universe,² such as the coma cluster (Jiménez-Teja et al. 2019), low metallicity stars (Whitten et al. 2019; Galarza et al. 2022), and galaxy formation (Nogueira-Cavalcante et al. 2019). J-PLUS has 12-waveband photometry, which makes the survey ideal for the application of machine learning.

In this study, we adopt the SVR algorithm to obtain the stellar parameters, which include the effective temperature (T_{eff}), the surface gravity ($\log g$), and the metallicity ($[\text{Fe}/\text{H}]$) of the stars in the J-PLUS DR1 catalog. To construct the training sample, we use data from LAMOST, the Apache Point Observatory Galactic Evolution Experiment (APOGEE, Zasowski et al. 2013), and the Sloan Extension for Galactic Understanding and Exploration (SEGUE, Yanny et al. 2009; Sect. 2).

We adopt the SVR (Awad & Khanna 2015; Drucker et al. 1997; Cortes & Vapnik 1995) algorithm and determine the kernel

scales (Sect. 3.1). We construct 80 training sets based on the uncertainties of the stellar parameters. Each parameter of any object in the 80 sets obeys a Gaussian distribution (Sect. 3.2). In all, we construct more than two hundred different models. The blind test is presented in Sect. 3.3.

The result of applying our method to the entire J-PLUS DR1 catalog is presented in Sect. 4. In Sect. 5.1 and 5.2, we compare different methods for constructing the training sample and the inconsistency of stellar parameters among different pipelines (Sect. 5.3). We discuss the distribution of the regressed stellar parameters in Sect. 5.4, and compare our result with Yang et al. (2021) in Sect. 5.5. We present a conclusion in Sect. 6.

2. Data

2.1. J-PLUS

J-PLUS is conducted by the Observatorio Astrofísico de Javalambre (OAJ, Teruel, Spain; Cenarro et al. 2014). It uses the 83 cm Javalambre Auxiliary Survey Telescope (JAST80) and T80Cam, which is a panoramic camera of $9.2\text{k} \times 9.2\text{k}$ pixels that provides a 2 deg^2 field of view (FoV) with a pixel scale of $0.55 \text{ arcsec pix}^{-1}$ (Marín-Franch et al. 2015). The J-PLUS contains a 12-passband filter system that comprises five broad (u, g, r, i, z) and seven medium bands from 3000 to 9000 Å. Cenarro et al. (2019) illustrate the scientific goals and the observational and image reduction strategy of J-PLUS.

J-PLUS DR1 covers an area of $1,022 \text{ deg}^2$ on the sky with a magnitude limit of ~ 21.5 for a S/N of ~ 3 . These 12 bands provide a large sample for us to characterize the spectral energy distribution of the detected sources (Cenarro et al. 2019). The 12-band magnitudes are adopted as our training features, which are $u, J0378, J0395, J0410, J0430, g, J0515, r, J0660, i, J0861,$ and z . We name them mag1 to mag12 for simplicity.

Yuan (2021) recalibrated the J-PLUS DR1 catalog using stellar color regression. The method is described in detail in Yuan et al. (2015). The catalog in Yuan (2021) contains 13,265,168 objects, including 4,126,928 objects with all 12 magnitudes. In Wang et al. 2021, the objects in the recalibrated J-PLUS catalog are classified using the support vector machine (SVM) algorithm, which distinguishes them among the classes STAR, GALAXY, and QSO. Here they chose the 12 J-PLUS magnitudes as features and used their corresponding uncertainties as weight for the SVM. They provide two catalogs based on the 12 density contours on the 12 magnitudes of the training sample. The objects that fall into all the 12 contours are assigned as interpolations, and the others are assigned as extrapolation. Interpolations have better classification accuracy than extrapolations. In this study, we use all objects classified as STAR in these two catalogs for the stellar parameter regressions.

2.2. LAMOST spectra

LAMOST is a northern spectroscopic survey situated at Xinglong Observatory, China. LAMOST is able to observe 4,000 objects simultaneously with a 20 deg^2 FoV. The main scientific project of LAMOST aims to understand the structure of the Milky Way (Deng et al. 2012) and external galaxies. We used the A, F, G, and K catalogs in LAMOST Data Release 7 (DR7), low resolution spectra (LRS), and medium resolution spectra (MRS)³.

³ <http://dr7.lamost.org/catalogue>

¹ http://J-PLUS.es/datareleases/data_release_dr2

² <http://J-PLUS.es/survey/science>

LAMOST LRS have a limiting magnitude of about 20 in the g band and its S/N is higher than 6 on dark nights or 15 on bright nights. In MRS, the S/N is always larger than 10. The parameters are given by the LAMOST Stellar Parameter pipeline (LASP), and their uncertainties are mainly from the stellar S/N and chi-square of the best-matched theoretical spectrum (Wu et al. 2014; Liu et al. 2020). The parameter differences of the LRS data and MRS data are very small, on average 17.6 K for T_{eff} , 0.028 dex for $\log g$ (g in cm s^{-2}), and 0.084 dex for $[\text{Fe}/\text{H}]$, according to our test. The internal uncertainties of LASP are estimated to be $\Delta T_{\text{eff}} \sim 80\text{K}$, $\Delta \log g \sim 0.15\text{dex}$, and $\Delta[\text{Fe}/\text{H}] \sim 0.09\text{dex}$ (Wang et al. 2020). We cross-matched these catalogs with J-PLUS DR1 to within one arcsec using the Tool for OPERations on Catalogues And Tables (TOPCAT, Taylor 2005). There are 216,114 and 25,170 cross-matched stars in the LRS and MRS catalogs, respectively.

2.3. APOGEE

APOGEE (Zasowski et al. 2013) has observed about 150,000 stars in the Milky Way and obtained precise stellar information, including stellar atmospheric parameters and radial velocities. The APOGEE Stellar Parameter and Chemical Abundance Pipeline (ASPCAP, García Pérez et al. 2016) uses a chi-square minimization to determine the stellar parameters. ASPCAP has high precision in stellar parameters ($\Delta T_{\text{eff}} \sim 2\%$, $\Delta \log g \sim 0.1\text{dex}$, and $\Delta[\text{Fe}/\text{H}] \sim 0.05\text{dex}$). Jönsson et al. (2018) compared the spectra and determined the uncertainties of the stellar parameters ($\Delta T_{\text{eff}} \sim 100\text{K}$, $\Delta \log g \sim 0.2\text{dex}$, and $\Delta[\text{Fe}/\text{H}] \sim 0.1\text{dex}$).

We adopted the APOGEE catalog to enlarge our training sample. Using the Sloan Digital Sky Survey (SDSS) Catalog Archive Server Jobs⁴, we extracted table `aspcapStar` and find 12,931 stars that satisfy our one arcsec cross-match tolerance.

2.4. SEGUE

SEGUE (Yanny et al. 2009) is designed to obtain images in the u , g , r , i , and z wavebands for 3,500 square degrees of the sky located primarily at low galactic latitudes ($|b| < 35^\circ$). It delivers observations of about 240,000 stars with a g band magnitude between 14.0 and 20.3 mag and moderate-resolution spectra from 3,900 to 9,000 Å. The stellar parameters are presented in SDSS Data Release 7 for these Milky Way stars with S/N greater than ten. The SEGUE Stellar Parameter Pipeline (SSPP; Lee et al. 2008a,b; Allende Prieto et al. 2008) developed a multi-method technology to calculate the stellar parameters which includes non-linear regression models, a minimal distance of observed spectra and grids of synthetic spectra, and the correlations between spectral lines and color relations. The average uncertainties of SSPP are $\Delta T_{\text{eff}} \sim 130\text{K}$, $\Delta \log g \sim 0.21\text{dex}$, and $\Delta[\text{Fe}/\text{H}] \sim 0.11\text{dex}$. One arcsec tolerance cross-match yields 25,487 stars.

2.5. RAVE

Bai et al. (2018) adopted the RAdial Velocity Experiment (RAVE, Steinmetz et al. 2020) catalog for their training sample. Our one arcsec tolerance cross-matching returns only 70 stars. Moreover, the RAVE catalog includes $[\text{m}/\text{Fe}]$ not $[\text{Fe}/\text{H}]$. The conversion from $[\text{m}/\text{Fe}]$ to $[\text{Fe}/\text{H}]$ could import bias or deviation when using an empirical formula. Therefore, the RAVE catalog is not included in our training sample.

2.6. Normalization

The training sample was constructed with J-PLUS DR1 and three spectral surveys, 12,931 stars from APOGEE, 216,114 from LAMOST LRS, 25,170 from LAMOST MRS, and 25,487 from SSPP. After removing the stars with missing photometric observations in one or more bands, there are 279,702 stars left.

Prior to training our model, we centered all parameters x_i in our training data (both the targets and input magnitudes) by subtracting their mean: $x_{i,t} = x_i - E(x_i)$ ⁵. This normalization reduces the upper and lower bound of the parameter distribution and makes them all zero-mean distributed, which can accelerate the training speed (Shalev-Shwartz & Ben-David 2014).

During the prediction procedure, the query input magnitudes are centered in the same fashion, using the respective means from the training data, before being fed to the model. The model output $x_{i,p}^*$ is then returned to the true target parameter space following: $x_{i,p} = x_{i,p}^* + E(x_i)$ to retrieve the prediction $x_{i,p}$.

We kept the parameters of the same stars from different spectroscopy surveys. For example, star A appears in both LAMOST and APOGEE, and the corresponding effective temperatures are $T_{\text{eff}1}$ and $T_{\text{eff}2}$. In our sample set, there would be a star A_1 with effective temperature $T_{\text{eff}1}$ and another star A_2 with $T_{\text{eff}2}$. The stellar parameters are only merged when all parameters are the same.

2.7. Contours

The prior distributions of the parameters in the training sample set are shown in Appendix A. The effective temperature is mostly distributed from 5000 ~ 6000K, with $\log g$ about 4 ~ 4.8 and a metallicity similar to that of our Sun, which means that most stars are in their main sequence stage. There are also some giants with lower surface gravity (2 ~ 3), lower metallicity (< -1), and lower effective temperature (4000 ~ 5000K).

However, the LAMOST stellar parameters are extracted from the spectra whose S/N is higher than 10. This criterion makes our LAMOST sample brighter than the limit magnitude of J-PLUS stars. Such disagreement would decrease the accuracy of prediction. To solve this problem, we applied the method to control the interpolation and extrapolation in Wang et al. (2021). This method could increase the precision in prediction. To quantify the density of the sample space, we considered 12 sub-space combinations, which are (mag1, mag2, mag3), ..., (mag10, mag11, mag12), (mag11, mag12, mag1), and (mag12, mag1, mag2), and calculated the 95% density contours to make clear how they cycle through the parameter space. The sample space can be approached by the intersection space inside all these twelve density contours. Stars situated in all contours are assigned as interpolations.

3. Methodology

3.1. Support vector regression

The SVR (Awad & Khanna 2015; Drucker et al. 1997; Cortes & Vapnik 1995) algorithm is a regression method based on the SVM (SVM, Cortes & Vapnik 1995; Boser et al. 1992; Cristianini & Shawe-Taylor 2000; Shalev-Shwartz & Ben-David 2014). The data located inside the margin given by SVR algorithm are not involved in the calculation. These data gave us the flexibility to define the tolerance in regression.

⁵ E stands for mathematical expectation.

⁴ <http://skyserver.sdss.org/casjobs/>

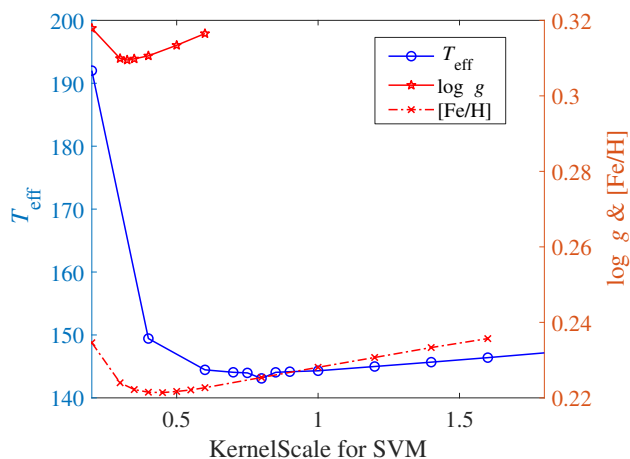


Fig. 1. RMSEs of the stellar parameters vs. the kernel scale. The blue line is the effective temperature. The surface gravity is the red solid line with the star markers, and the metallicity is the dotted line with the cross markers.

For a nonlinear regression problem, we first embedded the sample space into a new feature space with a higher dimension and transformed it into a linear regression problem. To transform the problem to the higher dimensional feature space, the SVR algorithm makes use of the kernel trick, which represents the inner product of the image of objects mapped from the sample space to the feature space with a kernel function. This process can accelerate the calculation by doing calculations in a lower dimension. In the feature space, the algorithm then fits the data linearly.

Similar to the SVM algorithm, the SVR also has a strip area (called a tube). The difference between the two algorithms is that SVM maximizes the minimal distance between each sample to the strip, while the SVR considers how to minimize the width of the strip to put all samples in. The width of the strip area is called the margin. The vectors from the final line to the samples that finally determined the strip area are called the support vector. Details on the algorithm are given in Smola & Schölkopf (2004).

The root mean square error (RMSE) is one of the most useful standards for evaluating the efficiency of regression. The RMSE of θ is given by $\sqrt{\mathbb{E}((\hat{\theta} - \theta)^2)}$, where $\hat{\theta}$ is the estimate of θ . In regression, the RMSE is given by

$$\text{RMSE} = \sqrt{\frac{1}{n} \sum_{t=1}^n (\hat{y}_t - y_t)^2},$$

where y is the stellar parameter.

In the pre-training, we tested both magnitudes and colors as the input features with the same preprocessing. As a result, the RMSE of the magnitudes was lower than that of the $\text{mag}(n-1) - \text{mag}(n)$ color under the default setting of SVR training (with Gaussian kernel 0.83). Then, we constructed independent models with different Gaussian kernel scales for each stellar parameter. We present the RMSE as a function of different kernel scales in Fig. 1. We used the kernel scales with the lowest RMSEs for the training. We also tested the $\text{mag}(n-1) - \text{mag}(n)$ and $\text{mag}1 - \text{mag}(n)$ color (Yang et al. 2021), and optimized the kernel scale with the Bayesian optimizer. Table 1 presents the adopted kernel scales and the corresponding RMSEs, which are based on ten-fold validation. We adopted 0.8 as the kernel scale of T_{eff} , 0.325 as the kernel scale of $\log g$, and 0.45 as the kernel scale of $[\text{Fe}/\text{H}]$.

3.2. Data enhancement

We duplicated the sample into 80 sets to enhance the cardinality of data for each stellar parameter. In image recognition, the method is usually carried out by rotating or mirroring the image and producing more samples for the training. We applied this method here by generating random training sets to fully use the uncertainties of both the magnitudes and the stellar parameters.

For each star in our training sample, after the centering process, we generated 80 stars with its 12 magnitudes, 3 stellar parameters, and 15 corresponding uncertainties. These 80 stars have Gaussian distributions of all the magnitudes and the stellar parameters following $\widetilde{x}_{i,t} = x_{i,t} + \sigma(x_{i,t})e_i$, where $\sigma(x_{i,t})$ is the uncertainty of $x_{i,t}$, and $\sigma_i \sim \text{N}(0, 1)$. For example, the mean temperature is 6,000K and the σ is 100K for the star with $T_{\text{eff}} = 6000 \pm 100\text{K}$. The simulation process did not change the original distribution or introduce new errors (Appendix A).

Each of the 80 constructed samples has 251,732 stars. We trained 80 models using the SVR algorithm with the same kernel scale in Sect. 3.1 for each stellar parameter, which resulted in a total of 240 different models (same scheme but different sample set) for T_{eff} , $\log g$, and $[\text{Fe}/\text{H}]$. We then used the corresponding 80 regression models to retrieve a distribution of 80 predictions for a given query observation. Then, we used Gaussian functions to fit these predicted distributions to obtain the centers and standard deviations.

The data enhancement method takes the uncertainties of stellar parameters into account, which are not considered in other studies. The absence of these uncertainties could cause unexpected errors in the prediction since the spectral precision is not involved in the model construction.

3.3. Model validation

We applied model validation to illustrate the effectiveness and to avoid potential overfitting. A widespread method for model validation is blind tests, which can reveal potential overfitting and quantify a model's ability to generalize to new, previously unseen data. We reserved 10%, 27,970 stars as our blind test sample, producing 80 sets of tests for each stellar parameter according to our data enhancement procedure. Similar to the construction of the sample set, we did not use any criterion to preselected data in order to avoid the selection effect.

We provide the RMSE and normalized RMSE (NRMSE) of our blind test for both interpolation and extrapolation in Table 2, where the $\text{NRMSE} = \frac{\sqrt{\sum_{i=1}^n (\hat{x}_i - x_i)^2}}{\max(x_i) - \min(x_i)}$. The prediction has the best result in effective temperature and the least in surface gravity. The extrapolation contains 445 stars, which suffered from a large deviation in the blind test. The result shows that the training model is better restricted in the space in which the samples are densely distributed.

Figure 2 shows the T_{eff} distribution of one star (26109-16130) in our blind tests. After applying the Lilliefors test (Lilliefors 1967), the p -value of the distribution is 0.375, greater than 0.05, implying that it may follow a Gaussian distribution. However, this may not generally be the case (Section 5.4). The results of the blind tests for $\log g$ and $[\text{Fe}/\text{H}]$ are presented in Appendix B.

4. Result

We then applied 240 stellar parameter models to the interpolation and extrapolation catalogs from Wang et al. (2021), sep-

Table 1. Adopted kernel scales and RMSEs.

	Kernel scale	Magnitude	Kernel Scale C1	Color1	Kernel Scale C2	Color2
T_{eff}	0.8	144.059	1.01	165.71	5.77	195.77
$\log g$	0.325	0.310	1.646	0.312	0.415	0.316
[Fe/H]	0.45	0.221	1.944	0.233	0.440	0.233

Notes. The "Magnitude" column lists the RMSE of using magnitudes as features, while the column of "Color1" is the $\text{mag}(n-1) - \text{mag}(n)$ color and "Color2", presents the optimized $\text{mag}1 - \text{mag}(n)$ color.

The 'Kernel Scale' columns match the magnitudes, color1, and color2, respectively.

Table 2. Blind test RMSEs

	BT RMSE	BT NRMSE	Inter RMSE	Inter NRMSE	Extra RMSE	Extra NRMSE
T_{eff}	159.6	0.0283	150.2	0.0266	454.0	0.0805
$\log g$	0.3453	0.0677	0.3380	0.0663	0.6543	0.1283
[Fe/H]	0.2503	0.0484	0.2428	0.0470	0.5402	0.1045

Notes. Inter stands for the interpolation and Extra stands for the extrapolation.

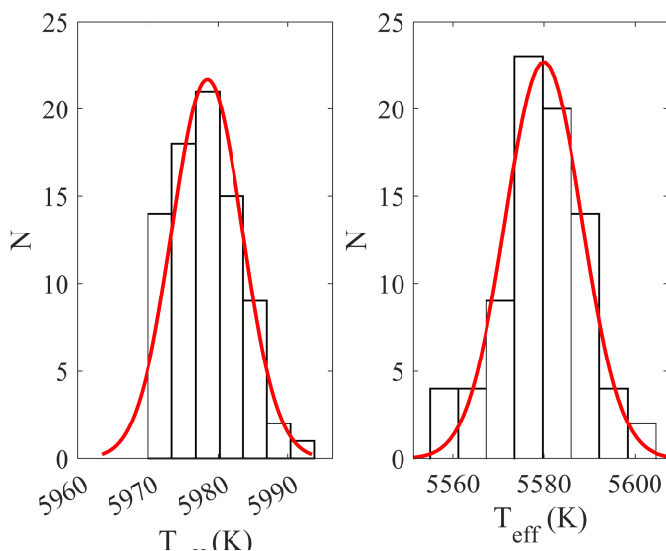


Fig. 2. Two examples of the T_{eff} distributions. The left panel is the distribution of T_{eff} of 26109-16130 in the blind test. The right panel is the distribution of 26016-295 in the prediction. The red lines are Gaussian fits.

arating our predictions into two catalogs. There are 2,493,424 objects in the interpolation catalog and 233,924 objects in the extrapolation catalog. In the classification, the authors restrained the 12-band magnitudes and constructed 12 contours based on the sample set distribution. All classified objects were assigned to the area inside or outside the contours and categorized as either interpolation or extrapolation. The distribution of inside objects is similar to the samples and therefore they have higher accuracy. In short, the stars in the interpolation catalog have a higher classification confidence than those in the extrapolation catalog.

We also applied this method in the prediction. There are 1,898,154 stars situated in our training set contours, and 595,270 stars are categorized as extrapolation in the classification interpolation catalog. In the classification extrapolation catalog, there are 13,274 interpolations and 220,650 extrapolations. We then input the 12-band magnitudes of each star into the 3×80 models

and obtained the stellar parameters of the interpolation and extrapolation catalogs. An example of the Gaussian fit is given in the right panel of Fig. 2. Table 3 is a stellar parameter catalog of the interpolation catalog.

Both median and mean values of the uncertainties are presented in Table 4. The difference in mean versus median shows the existence of a few stars with a large residual that raise the mean in both the interpolation and extrapolation catalogs. These uncertainties were decreased by about 3% ~ 5% by applying the contours to constrain the prediction sample. The uncertainties of the prediction are smaller than the residuals among different pipelines, implying that our regressions have fairly good precisions (see Sect. 5.3). This also implies that the uncertainties are mainly generated from the pipeline difference and observation uncertainties.

5. Discussion

5.1. Training and blind test

We tested three methods to regress the parameters. In the first method, we trained a single SVR model using the magnitude uncertainties as weights, but excluding the stellar parameter uncertainties. This method aims at making a comparison with our multi-model simulation. The weight is given by $w_i = \lg \sum_{j=1}^1 2(\frac{1}{e_{ij}})$ for an object x_i , where the e_{ij} shows the magnitude uncertainty of $\text{mag}j$. We adopted a logarithmic scale to reduce potential steep cliffs in the feature space (Wang et al. 2021). In the second and third tests, we randomly constructed 80 training sets for each stellar parameter. The difference between the two tests is whether LAMOST MRS were included in the training sample. We constructed the second test to show the generalization ability of extrapolating data. The first and second tests use LAMOST MRS as a blind test, while the third one includes all the stars in the training sample and holds 10% for the blind test. The third method is the final model we applied. It has lower RMSEs than the single model. We present the results of these three tests in Table 5.

Table 3. Parameter catalog of the interpolation

ID	R.A. (deg)	Dec. (deg)	T _{eff} (K)	ΔT _{eff} (K)	log <i>g</i> (dex)	Δlog <i>g</i> (dex)	[Fe/H] (dex)	Δ[Fe/H] (dex)
26016-5*	255.4683	22.7600	6831	101	3.71	0.14	-1.20	0.10
26016-15	255.3051	22.7608	5950	15	4.15	0.07	-0.36	0.04
26016-16*	255.3675	22.7611	5659	127	3.89	0.08	-0.79	0.10
26016-50*	255.1639	22.7644	6034	80	3.71	0.13	-1.19	0.17
26016-55*	255.6631	22.7617	4061	120	3.93	0.06	-0.67	0.09
26016-64*	254.7562	22.7650	6175	58	3.73	0.13	-1.18	0.15
26016-68	255.7539	22.7623	6467	13	3.59	0.07	-1.63	0.06
26016-70	255.3743	22.7649	6137	41	3.54	0.14	-1.62	0.10
26016-74	255.5894	22.7630	6162	14	3.87	0.06	-1.04	0.05
26016-84*	254.8371	22.7663	5532	151	3.84	0.04	-0.76	0.09

Notes. ID stands for the J-PLUS ID. RA and Dec. are the right ascension and the declination in degree (J2000). The extrapolation stars have an asterisk on their ID, which indicates that their stellar parameters are not very reliable. The Δ shows the uncertainty.

Table 4. Uncertainties of the classification interpolation and the extrapolation catalogs

	Inter median	Inter mean	Extra median	Extra mean
T _{eff} (K)	14.0	34.7	59.5	71.6
log <i>g</i> (dex)	0.0689	0.0780	0.0268	0.0515
[Fe/H] (dex)	0.0566	0.0677	0.0187	0.0477

Notes. Inter stands for the classification interpolation catalog and Extra stands for the classification extrapolation catalog. We present both median and mean values in this table.

Table 5. RMSEs of the blind tests in the three tests

Method	T _{eff} (K)	log <i>g</i> (dex)	[Fe/H] (dex)
Single Model	239.9	0.373	0.296
Generalization Ability	239.6	0.400	0.313
Final Model	159.6	0.345	0.250

5.2. Multi-model approach

Bai et al. (2018) constructed a single model to train the stellar parameters and enlarge the sample to constrain the discrepancy caused by different pipelines. The uncertainty of the stellar parameter is not included in their calculation. Yang et al. (2021) also constructed one deep learning artificial neural network (ANN) — *CSNet* — and gained stellar parameters with a precision of ~ 55 K in effective temperature, 0.15 dex in log *g*, and 0.07 dex in [Fe/H]. Galarza et al. (2022) presented a multi-regressor pipeline, SPEEM, based on three single XGB algorithms and validated the result with SSPP. The errors for each stellar parameter (T_{eff}, log *g*, [Fe/H]) are 41 ± 61 K, 0.11 ± 0.17 dex, and 0.09 ± 0.14 dex, respectively. More information is presented in Table 6. The precision of all these single models is similar to our results.

In our study, the RMSE of a single model is similar to the RMSEs of 80 models, indicating that the multi-model approach performs similarly to the weight-controlled model. We can incorporate the uncertainties of both features and target parameters, which is the main advantage of our approach. Furthermore, if a certain photometric measurement suffers a higher uncertainty, its contribution to the regression would decrease significantly, independently of the uncertainties in the remaining 11 measurements. This could introduce biases into the models and result in inaccurate predictions. Such bias is avoided in our re-

sults, since all the uncertainties of the 12-band magnitudes are included in the model construction.

We also find that the uncertainties of the stellar parameters are larger than the blind test’s RMSEs. If these uncertainties are not considered in the calculation, the error from the spectral fitting pipeline would not propagate to the final regression. The uncertainties of the prediction would be highly underestimated in this case.

5.3. Pipelines

Different pipelines result in different stellar parameters (Fig. 3, see more in Appendix C), and we adopted all parameters from all pipelines. We selected the stars that have parameters from multiple spectroscopy surveys and show the differences and variances in Table 7. In Table 6 and Table 7, the differences in the blind test are smaller than those caused by pipelines. When the stellar parameters from different pipelines are included in our training, the regression models are unbiased among these different pipelines and can thus be used to provide general predictions from different surveys. Including a larger variety of surveys in the training data will improve the generalization ability.

Other studies usually adopt data from one survey to avoid biases among different pipelines (Bu et al. 2020; Lu & Li 2015). Another method is to set a priority for each catalog. Some studies have concluded that a larger sample size can decrease the bias caused by pipelines, for example Bai et al. (2018).

Although a single catalog and priority-based methods do not suffer the systematic error caused by pipelines, the models built from them probably do not perform well for other surveys. Our training sample contains different surveys, and their biases propagate to the final regression models. Therefore, our models would have a wider application.

One catalog-based method may be good for regression of the same catalog, but J-PLUS is a more general catalog with a

Table 6. Gaussian fits of the residuals for our blind tests and other works.

Parameter	μ (BT)	Δ (BT)	Δ (Train)	Δ (Bai)	Δ (Yang)	μ (Galarza)	Δ (Galarza)
T_{eff} (K)	2.3125	159.5216	84.6750	100 ~ 200	~ 55	41	61
$\log g$ (dex)	0.0520	0.3413	0.1200		0.15	0.11	0.17
[Fe/H] (dex)	0.0366	0.2476	0.0660		0.07	0.09	0.14

Notes. BT stands for the blind test. Bai, Yang, and Galarza present the uncertainties from Bai et al. 2018, Yang et al. 2021, and Galarza et al. 2022, respectively. Bai et al. 2018 only contains effective temperature regression. μ is the center of the Gaussian fit and Δ is the standard deviation. We present the median values of the training uncertainties.

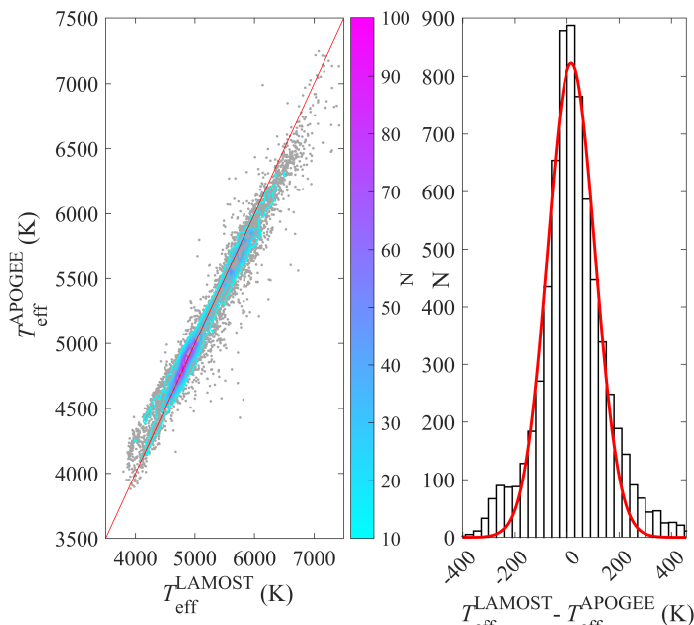


Fig. 3. One-to-one correlation of T_{eff} between APOGEE and LAMOST. Data points are in gray. The color bar is the density contours. The Gaussian fit of the residual is presented in the right panel. The mean of this normal distribution is -27.7873, and its standard deviation is 143.2126.

Table 7. Differences among pipelines

Stellar parameter	pipelines	overlap	μ	σ
T_{eff}	L–A	6,956	27.8	143.2
	L–S	3,318	-88.4	143.1
	S–A	64	-112.3	149.7
$\log g$	L–A		0.048	0.191
	L–S		0.206	0.353
	S–A		-0.150	0.228
[Fe/H]	L–A		0.008	0.099
	L–S		0.068	0.184
	S–A		-0.111	0.144

Notes. The mean and standard variance of the difference of pipelines. In this table, the "L" stands for LAMOST, while "S" for SSPP and "A" for APOGEE. Overlap stands for the number of cross-match overlapping between these catalogs. The unit of effective temperature is in K, and dex for $\log g$ and [Fe/H].

large sky coverage and many photometric wavebands. J-PLUS requires models from hybrid samples for general applications.

There may not exist a regressor that can properly fit the data for all the surveys; this is analogous to the no-free-lunch the-

orem, which says that a machine-learning algorithm that can solve every problem does not exist (Shalev-Shwartz & Ben-David 2014). This implies that the prediction would be biased if we use single catalog or priority-based methods to regress the data in another catalog. In machine learning, a larger amount of data does not always work, but higher diversity does (Wang et al. 2021).

5.4. Distribution of stellar parameters

While our data augmentation process employs Gaussian-based uncertainty sampling, the predicted stellar parameters may not necessarily follow a Gaussian distribution. The SVR embeds the samples to a higher-dimensional feature space by using a nonlinear embedding mapping. The nonlinear mapping may not hold the distribution of sample to the feature space.

To quantify whether our approach preserves the shape of the distribution, we applied the Lilliefors test (Lilliefors 1967) to the blind test samples. About 19.01% of the T_{eff} , 19.49% for $\log g$, and 19.39% for [Fe/H] pass the test with a significance level of 0.05. When the level decreases to 0.01, the number increases to 39.94% of the T_{eff} , 41.40% for $\log g$ and 40.54% for [Fe/H]. Given the low number statistics in our predicted distributions of only 80 samples, it is possible that this test underestimates the true fraction of Gaussian distributed predictions. To estimate the influence of the number of samples, we constructed 27,970 sets (which was the same size as the blind test size) of random numbers based on $N(100, 25)$ and find that about 94.87% passed the test with a significance level of 0.05. When we change the number of sets to 800, the result increases to 95.11%. The difference is less than 1%. Therefore, there is no evidence that the resulted stellar parameters follow a Gaussian distribution.

5.5. Comparison with Yang et al. (2021)

To determine the robustness of our predictions, we performed a comparison with the stellar parameter catalog from Yang et al. (2021)⁶. We selected the reliable stars in both catalogs, which were stars in the interpolation catalog and the stars with stellar parameter FLAG=0 in Yang et al. (2021). The cross-match yielded 2,008,654 stars. The average stellar parameter differences are -247.9764 K for T_{eff} , -0.1984 dex for $\log g$, and -0.0998 dex for [Fe/H]. There are some extreme values in Yang et al. (2021), and some of them are unreliable. For example, the maximum and minimum value of surface gravity are 882.44 dex and -237.24 dex and 460.39 dex and -567.16 dex for [Fe/H]. These stars may be situated at the edge of the feature space and, thus, are subject to overfitting by the ANN model.

⁶ available at http://www.j-plus.es/ancillarydata/dr1_stellar_parameters_elemental_abundances

The training sample ranges of Yang et al. (2021) are about 4000 ~ 7500 K for T_{eff} , 0 ~ 5 dex for $\log g$, and -3 ~ 1 dex for [Fe/H]. We restricted their results to these ranges and obtain 1,663,053 stars. The average differences decrease to -63.6817 K for T_{eff} , 0.0886 dex for $\log g$, and -0.1069 dex for [Fe/H] (Fig. 4). These differences are similar to our blind test uncertainties. The main difference between our work and Yang et al. (2021) is the control of the extrapolations. These extreme values might fall into the extrapolation category and suffer from overfitting. The training sample of Yang et al. (2021) is not an official LAMOST release, and the training sample difference may also be a minor reason for such a stellar parameter difference.

6. Conclusion

In this work, we predicted stellar parameters, the effective temperature T_{eff} , the surface gravity $\log g$, and the metallicity [Fe/H] for J-PLUS DR1 by using 3×80 SVR models. We chose stars from spectra-based surveys (LAMOST, APOGEE, and SEGUE) to construct our training sample in order to improve the reliability of the sample and gained 279,702 stars from the cross-match. We normalized the features of these stars by subtracting their average in order to accelerate the calculation. We held out ten percent of the set for the blind test and the remaining 251,732 stars were used for training. We used 12 three-dimensional density contours to distinguish the prediction reliability for a given star. We presented two catalogs that correspond to the classification catalogs of Wang et al. (2021). For the classification interpolation catalog, we present 1,898,154 stars with interpolated stellar parameters and 595,270 stars with extrapolations in our regression. For their classification extrapolation catalog, on the other hand, we present 13,274 interpolated and 220,650 extrapolated predictions with our SVR. Regarding the construction of the models, multi-model simulations give better results than the single model. The RMSEs of our validations are 159.6 for T_{eff} , 0.3453 for $\log g$, and 0.2502 for [Fe/H]. Using different catalogs as a sample set may increase the generalization ability of our model. Lastly, we compared our results to Yang et al. (2021) and find a decent agreement with their work, with discrepancies comparable to the RMSEs that we found in our blind test.

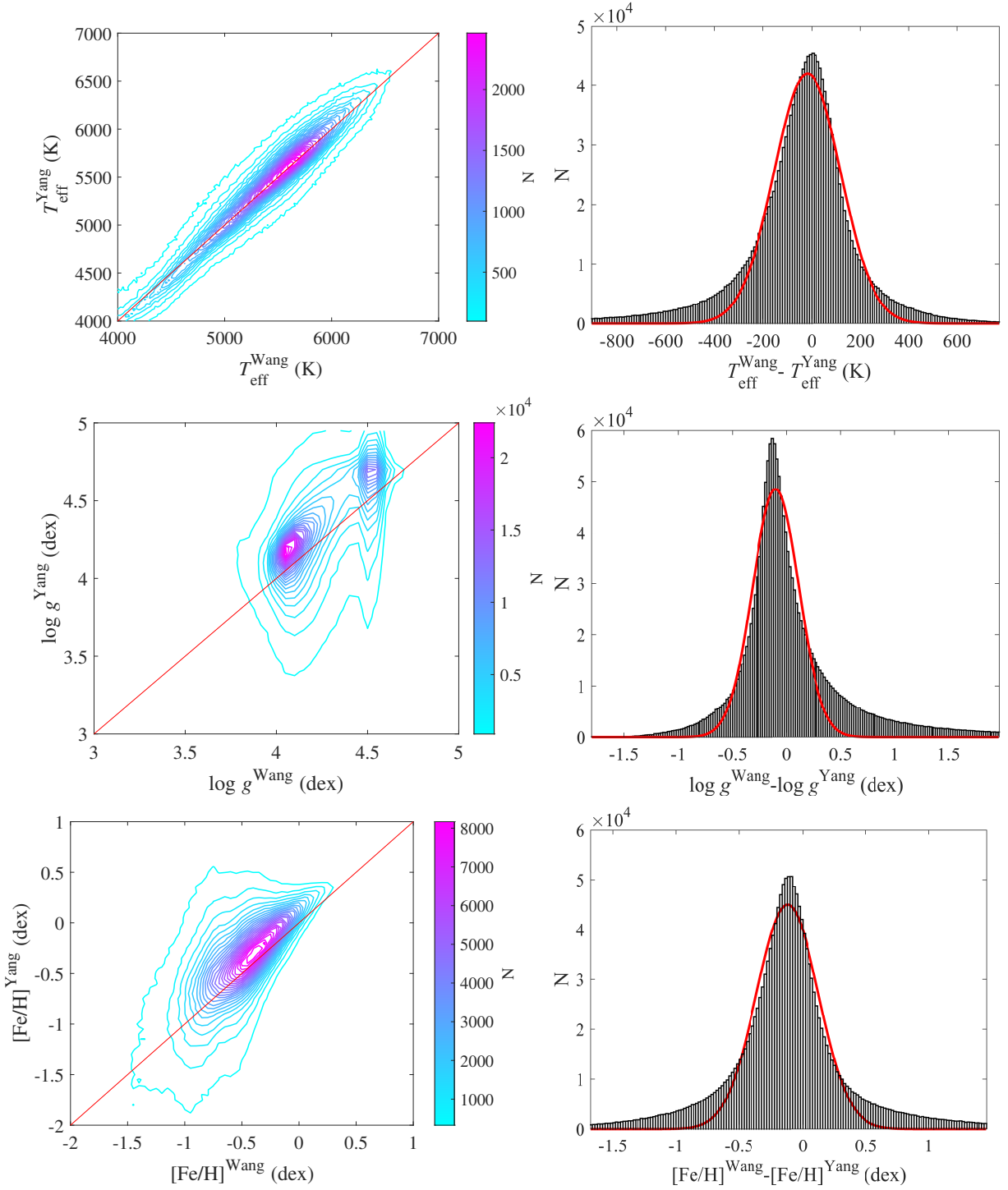


Fig. 4. Comparison with Yang et al. (2021). The three panels are T_{eff} , $\log g$, and $[\text{Fe}/\text{H}]$, from top to bottom. Only the density contours are shown in these figures.

Acknowledgements. This work was supported by the National Natural Science Foundation of China (NSFC) through grants NSFC-11988101/11973054/11933004 and the National Programs on Key Research and Development Project (grant No.2019YFA0405504 and 2019YFA0405000). Strategic Priority Program of the Chinese Academy of Sciences under grant number XDB41000000. H. B. Yuan, acknowledge funding from National Natural Science Foundation of China (NSFC) through grants NSFC-12173007. JAFO acknowledges the financial support from the Spanish Ministry of Science and Innovation and the European Union – NextGenerationEU through the Recovery and Resilience Facility project ICTS-MRR-2021-03-CEFCA. F.J.E. acknowledges financial support by the Spanish grant PGC2018-101950-B-I00 and MDM-2017-0737 at Centro de Astrobiología (CSIC-INTA), Unidad de

Excelencia María de Maeztu. We acknowledge the science research grants from the China Manned Space Project with NO.CMS-CSST-2021-B07.

Based on observations made with the JAST80 telescope at the Observatorio Astrofísico de Javalambre (OAJ), in Teruel, owned, managed, and operated by the Centro de Estudios de Física del Cosmos de Aragón (CEFCA). We acknowledge the OAJ Data Processing and Archiving Unit (UPAD) for reducing the OAJ data used in this work. Funding for the J-PLUS Project has been provided by the Governments of Spain and Aragón through the Fondo de Inversiones de Teruel; the Aragón Government through the Research Groups E96, E103, and E16_17R; the Spanish Ministry of Science, Innovation and Universities (MCIU/AEI/FEDER, UE) with grants PGC2018-097585-B-C21 and PGC2018-097585-B-C22; the Spanish Ministry of Economy and Compet-

itiveness (MINECO) under AYA2015-66211-C2-1-P, AYA2015-66211-C2-2, AYA2012-30789, and ICTS-2009-14; and European FEDER funding (FCDD10-4E-867, FCDD13-4E-2685). The Brazilian agencies FINEP, FAPESP, and the National Observatory of Brazil have also contributed to this project. Guoshoujing Telescope (the Large Sky Area Multi-Object Fiber Spectroscopic Telescope LAMOST) is a National Major Scientific Project built by the Chinese Academy of Sciences. Funding for the project has been provided by the National Development and Reform Commission. LAMOST is operated and managed by the National Astronomical Observatories, Chinese Academy of Sciences. Funding for the Sloan Digital Sky Survey IV has been provided by the Alfred P. Sloan Foundation, the U.S. Department of Energy Office of Science, and the Participating Institutions. SDSS-IV acknowledges support and resources from the Center for High-Performance Computing at the University of Utah. The SDSS website is <http://www.sdss.org/>. SDSS-IV is managed by the Astrophysical Research Consortium for the Participating Institutions of the SDSS Collaboration including the Brazilian Participation Group, the Carnegie Institution for Science, Carnegie Mellon University, the Chilean Participation Group, the French Participation Group, Harvard-Smithsonian Center for Astrophysics, Instituto de Astrofísica de Canarias, The Johns Hopkins University, Kavli Institute for the Physics and Mathematics of the Universe (IPMU)/University of Tokyo, Lawrence Berkeley National Laboratory, Leibniz Institut für Astrophysik Potsdam (AIP), Max-Planck-Institut für Astronomie (MPIA Heidelberg), Max-Planck-Institut für Astrophysik (MPA Garching), Max-Planck-Institut für Extraterrestrische Physik (MPE), National Astronomical Observatories of China, New Mexico State University, New York University, University of Notre Dame, Observatório Nacional/MCTI, The Ohio State University, Pennsylvania State University, Shanghai Astronomical Observatory, United Kingdom Participation Group, Universidad Nacional Autónoma de México, University of Arizona, University of Colorado Boulder, University of Oxford, University of Portsmouth, University of Utah, University of Virginia, University of Washington, University of Wisconsin, Vanderbilt University, and Yale University.

References

- Allende Prieto, C., Sivarani, T., Beers, T. C., et al. 2008, *AJ*, 136, 2070
- Anguiano, B., Majewski, S. R., Allende-Prieto, C., et al. 2018, *A&A*, 620, A76
- Awad, M. & Khanna, R. 2015, *Support Vector Regression* (Berkeley, CA: Apress), 67–80
- Bai, Y., Liu, J., Bai, Z., Wang, S., & Fan, D. 2019, *The Astronomical Journal*, 158, 93
- Bai, Y., Liu, J., Wang, S., & Yang, F. 2018, *The Astronomical Journal*, 157, 9
- Bailer-Jones, C. A. L. 2011, *Monthly Notices of the Royal Astronomical Society*, 411, 435
- Boeche, C., Smith, M. C., Grebel, E. K., et al. 2018, *The Astronomical Journal*, 155, 181
- Boser, B. E., Guyon, I. M., & Vapnik, V. N. 1992, in *Proceedings of the Fifth Annual Workshop on Computational Learning Theory, COLT '92* (New York, NY, USA: Association for Computing Machinery), 144–152
- Breiman, L. 2001, *Statist. Sci.*, 16, 199
- Bu, Y., Kumar, Y. B., Xie, J., et al. 2020, *The Astrophysical Journal Supplement Series*, 249, 7
- Cenarro, A. J., Moles, M., Cristóbal-Hornillos, D., et al. 2019, *Astronomy & Astrophysics*, 622, A176
- Cenarro, A. J., Moles, M., Marín-Franch, A., et al. 2014, in *Proc. SPIE*, Vol. 9149, *Observatory Operations: Strategies, Processes, and Systems V*, 914911
- Cortes, C. & Vapnik, V. 1995, *Machine Learning*, 20, 273
- Cover, T. & Hart, P. 1967, *IEEE Trans. Inf. Theory*, 13, 21
- Cristianini, N. & Shawe-Taylor, J. 2000, *An Introduction to Support Vector Machines and Other Kernel-based Learning Methods* (Cambridge University Press)
- Deng, L.-C., Newberg, H. J., Liu, C., et al. 2012, *Research in Astronomy and Astrophysics*, 12, 735
- Drucker, H., Burges, C. J., Kaufman, L., et al. 1997, *Advances in neural information processing systems*, 9, 155
- Galarza, C. A., Daflon, S., Placco, V. M., et al. 2022, *A&A*, 657, A35
- García Pérez, A. E., Allende Prieto, C., Holtzman, J. A., et al. 2016, *AJ*, 151, 144
- Jiménez-Teja, Y., Dupke, R. A., Lopes de Oliveira, R., et al. 2019, *Astronomy & Astrophysics*, 622, A183
- Jönsson, H., Prieto, C. A., Holtzman, J. A., et al. 2018, *The Astronomical Journal*, 156, 126
- Lee, Y. S., Beers, T. C., Sivarani, T., et al. 2008a, *AJ*, 136, 2022
- Lee, Y. S., Beers, T. C., Sivarani, T., et al. 2008b, *AJ*, 136, 2050
- Lilliefors, H. W. 1967, *Journal of the American Statistical Association*, 62, 399
- Liu, C., Fu, J., Shi, J., et al. 2020, *LAMOST Medium-Resolution Spectroscopic Survey (LAMOST-MRS): Scientific goals and survey plan*
- Lu, Y. & Li, X. 2015, *Monthly Notices of the Royal Astronomical Society*, 452, 1394
- MacKay, D. J. 2003, *Information theory, inference and learning algorithms* (Cambridge university press)
- Marín-Franch, A., Taylor, K., Cenarro, J., Cristóbal-Hornillos, D., & Moles, M. 2015, in *IAU General Assembly*, Vol. 29, 2257381
- Nogueira-Cavalcante, J. P., Dupke, R., Coelho, P., et al. 2019, *Astronomy & Astrophysics*, 630, A88
- Quinlan, J. R. 1986, *Machine Learning*, 1, 81
- Ruder, S. 2017, *An overview of gradient descent optimization algorithms*
- Shalev-Shwartz, S. & Ben-David, S. 2014, *Understanding Machine Learning: From Theory to Algorithms* (Cambridge University Press)
- Sichevskij, S. G. 2012, *Astronomy Reports*, 56, 710
- Sichevskij, S. G., Mironov, A. V., & Malkov, O. Y. 2014, *Astrophysical Bulletin*, 69, 160
- Smola, A. J. & Schölkopf, B. 2004, *Statistics and Computing*, 14, 199
- Steinmetz, M., Matijević, G., Enke, H., et al. 2020, *The Astronomical Journal*, 160, 82
- Stone, C. J. 1977, *The Annals of Statistics*, 5, 595
- Taylor, M. B. 2005, in *Astronomical Society of the Pacific Conference Series*, Vol. 347, *Astronomical Data Analysis Software and Systems XIV*, ed. P. Shopbell, M. Britton, & R. Ebert, 29
- Wang, C., Bai, Y., Yuan, H., Wang, S., & Liu, J. 2021, *Machine Learning Applied to STAR-GALAXY-QSO Classification of The Javalambre-Photometric Local Universe Survey*
- Wang, J., Fu, J.-N., Zong, W., et al. 2020, *The Astrophysical Journal Supplement Series*, 251, 27
- Whitten, D. D., Placco, V. M., Beers, T. C., et al. 2019, *Astronomy & Astrophysics*, 622, A182
- Wu, Y., Luo, A., Du, B., Zhao, Y., & Yuan, H. 2014, *Automatic stellar spectral parameterization pipeline for LAMOST survey*
- Wu, Y., Luo, A. L., Li, H.-N., et al. 2011, *Research in Astronomy and Astrophysics*, 11, 924
- Yang, L., Yuan, H., Xiang, M., et al. 2021, *arXiv e-prints*, arXiv:2112.07304
- Yanny, B., Rockosi, C., Newberg, H. J., et al. 2009, *The Astronomical Journal*, 137, 4377
- Yuan, H. 2021, *In preparation and private communication*
- Yuan, H., Liu, X., Xiang, M., et al. 2015, *The Astrophysical Journal*, 799, 133
- Zasowski, G., Johnson, J. A., Frinchaboy, P. M., et al. 2013, *The Astronomical Journal*, 146, 81

Appendix A: Sample

We present the distribution of a sample set in this section. The standard sample set distributions are shown in red blocks. We then split the sample set into 80 new randomly constructed sample sets to perform our simulation. The distribution contains all constructed objects of the 80 sets and is presented in the white block. The overlapping part of these blocks will fade to pink, and we can see that these figures are nearly all in pink.

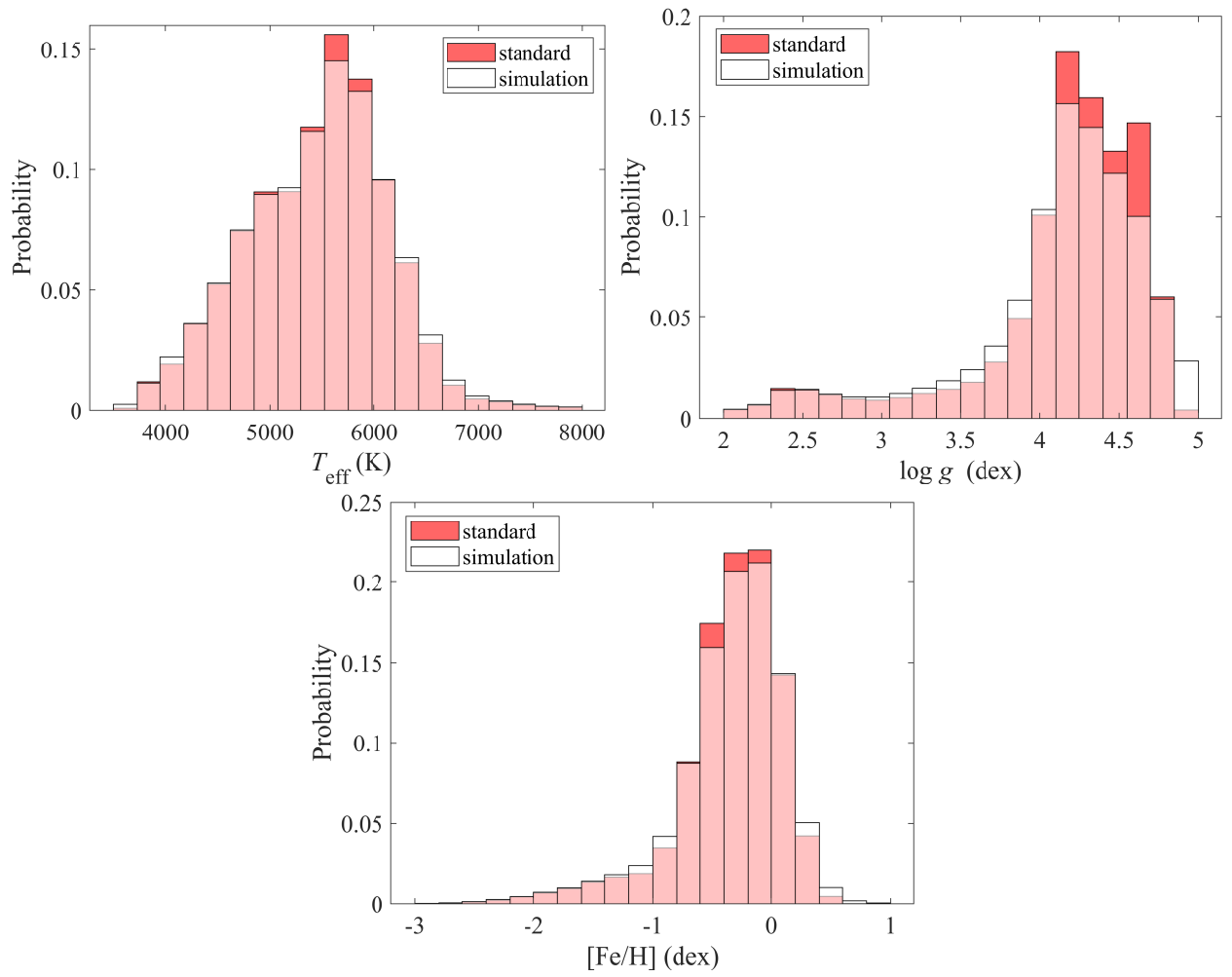


Fig. A.1. Stellar parameter distributions of the sample set. The red block shows the distribution of standard sample set. The white block shows the simulation distribution. The overlap is shown in pink (red+white). The y axis shows the probability.

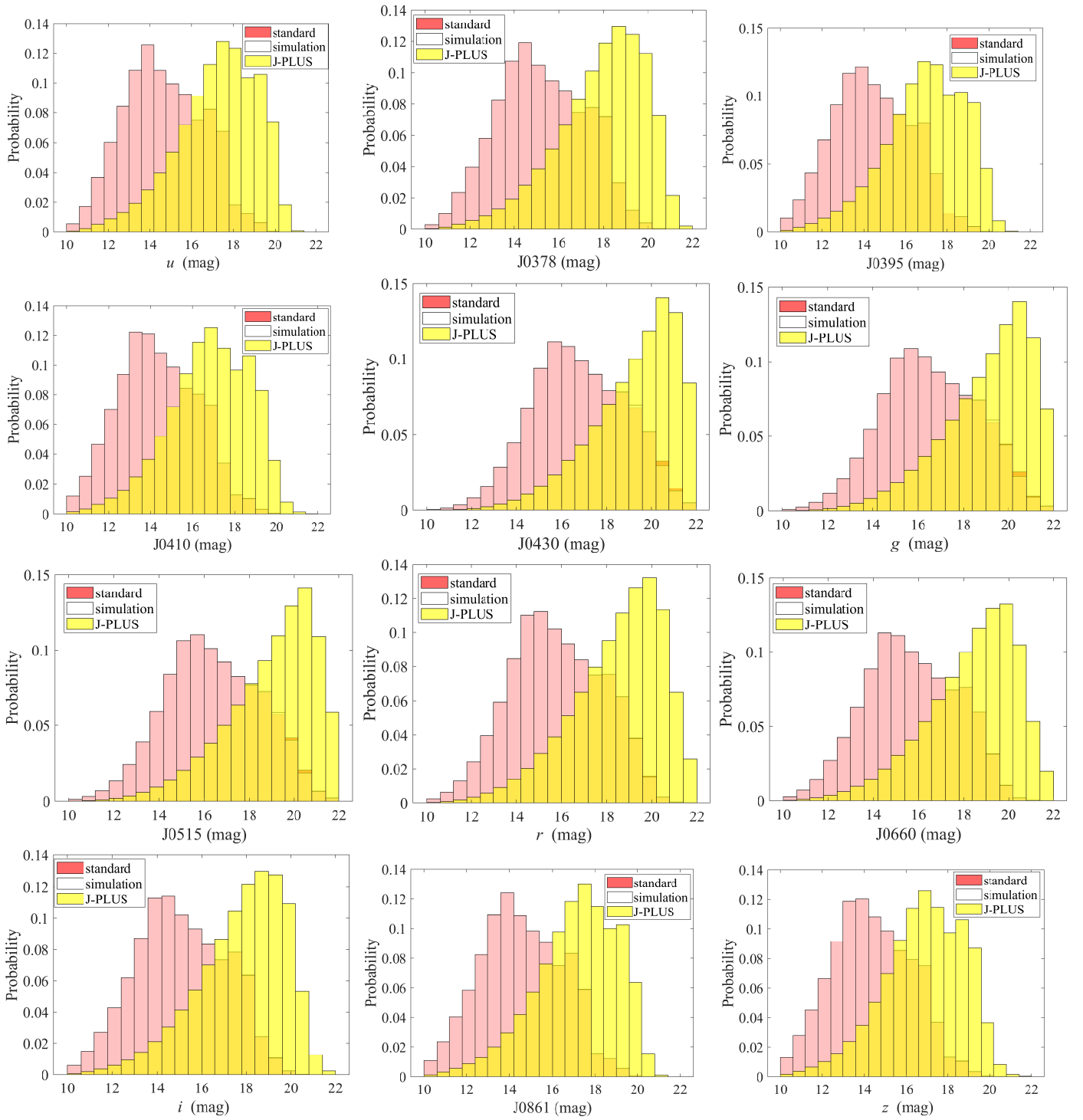


Fig. A.2. Magnitude distributions of the sample set. The yellow block shows the J-PLUS distribution.

Appendix B: Blind test result

We plot the results of the blind test, showing the differences between the predicted and the true parameters. We fit the residuals with Gaussian functions.

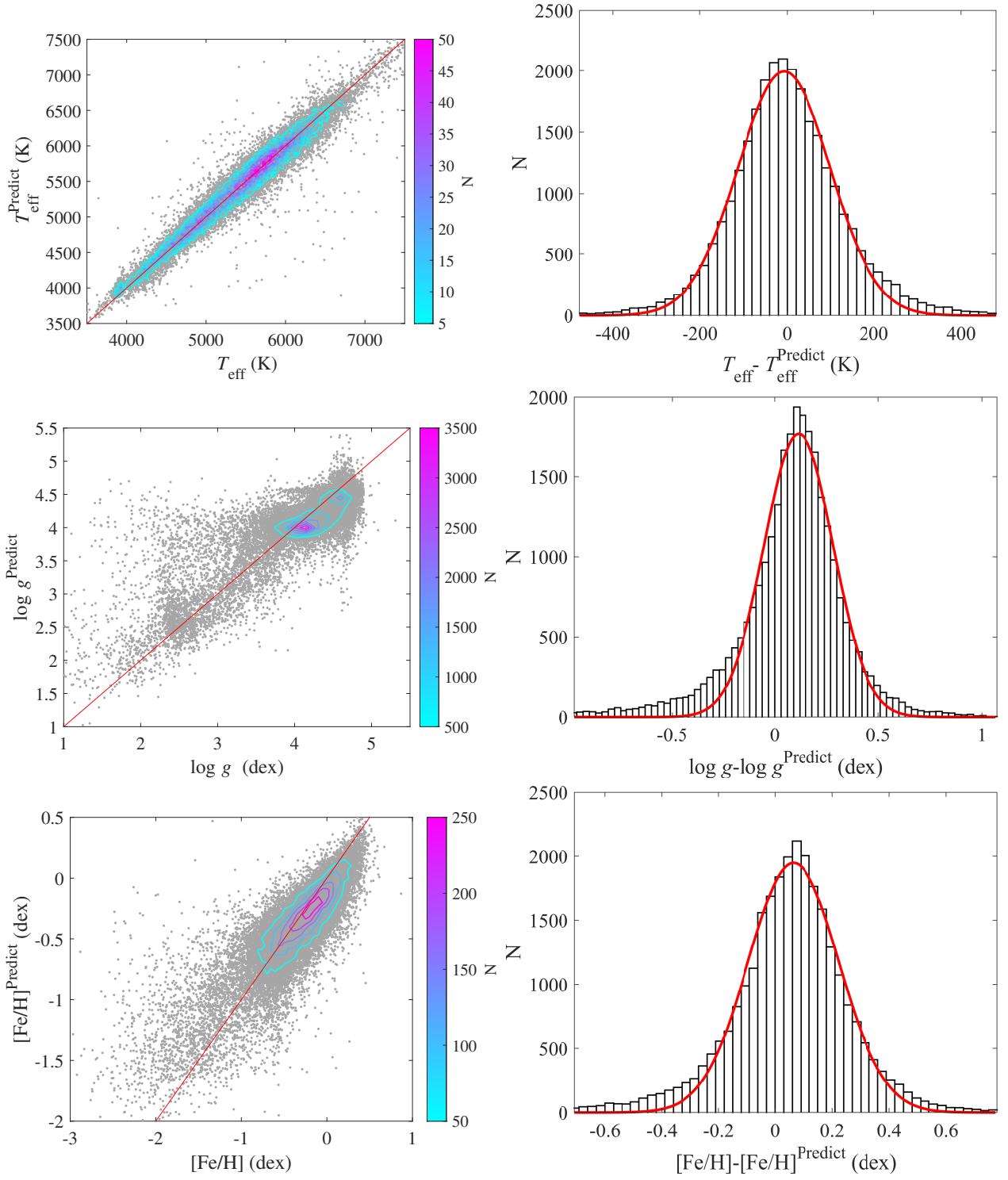


Fig. B.1. Results of the blind test validation. The upper two panels are T_{eff} . The middle two panels are $\log g$, and the lower two panels are $[\text{Fe}/\text{H}]$.

Appendix C: Pipeline differences

We present the differences among the pipelines. The residuals are fitted by Gaussian functions, and the means and variances are shown in Table 7.

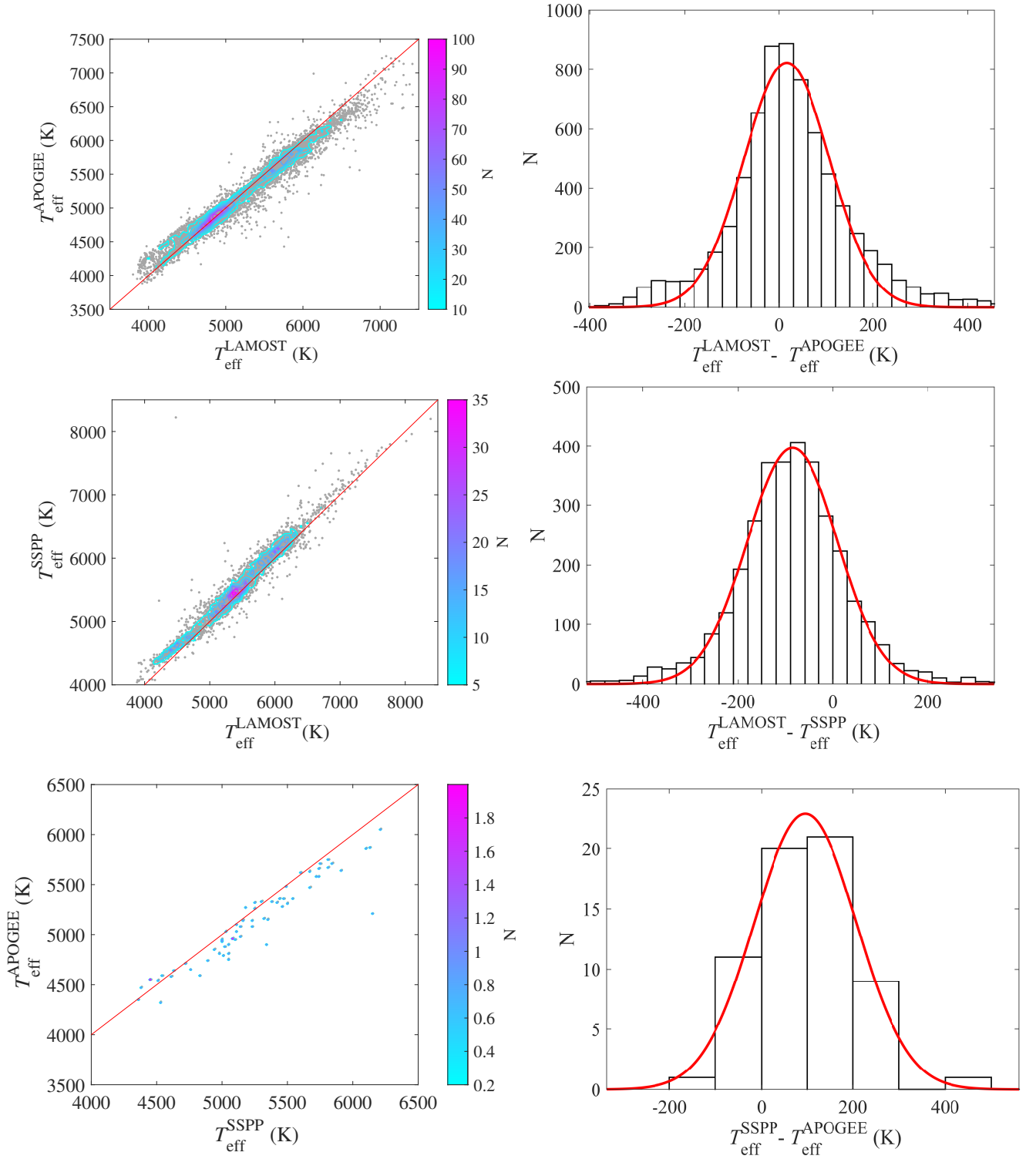


Fig. C.1. Pipeline differences of T_{eff} . The upper two panels show the difference between LAMOST and APOGEE. The middle two are the difference between LAMOST and SSPP, and the lower two are the difference between SSPP and APOGEE.

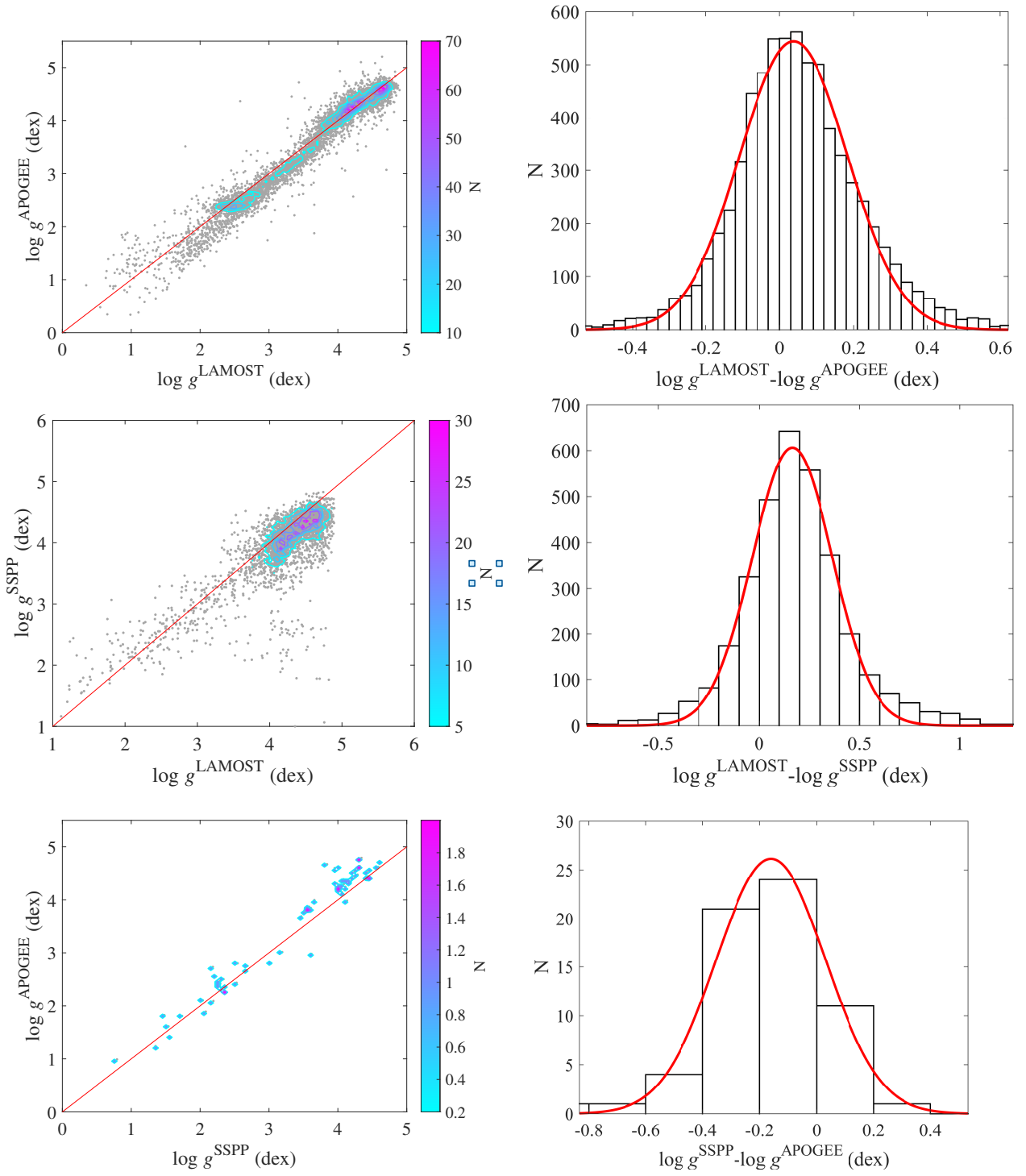


Fig. C.2. Pipeline difference of $\log g$.

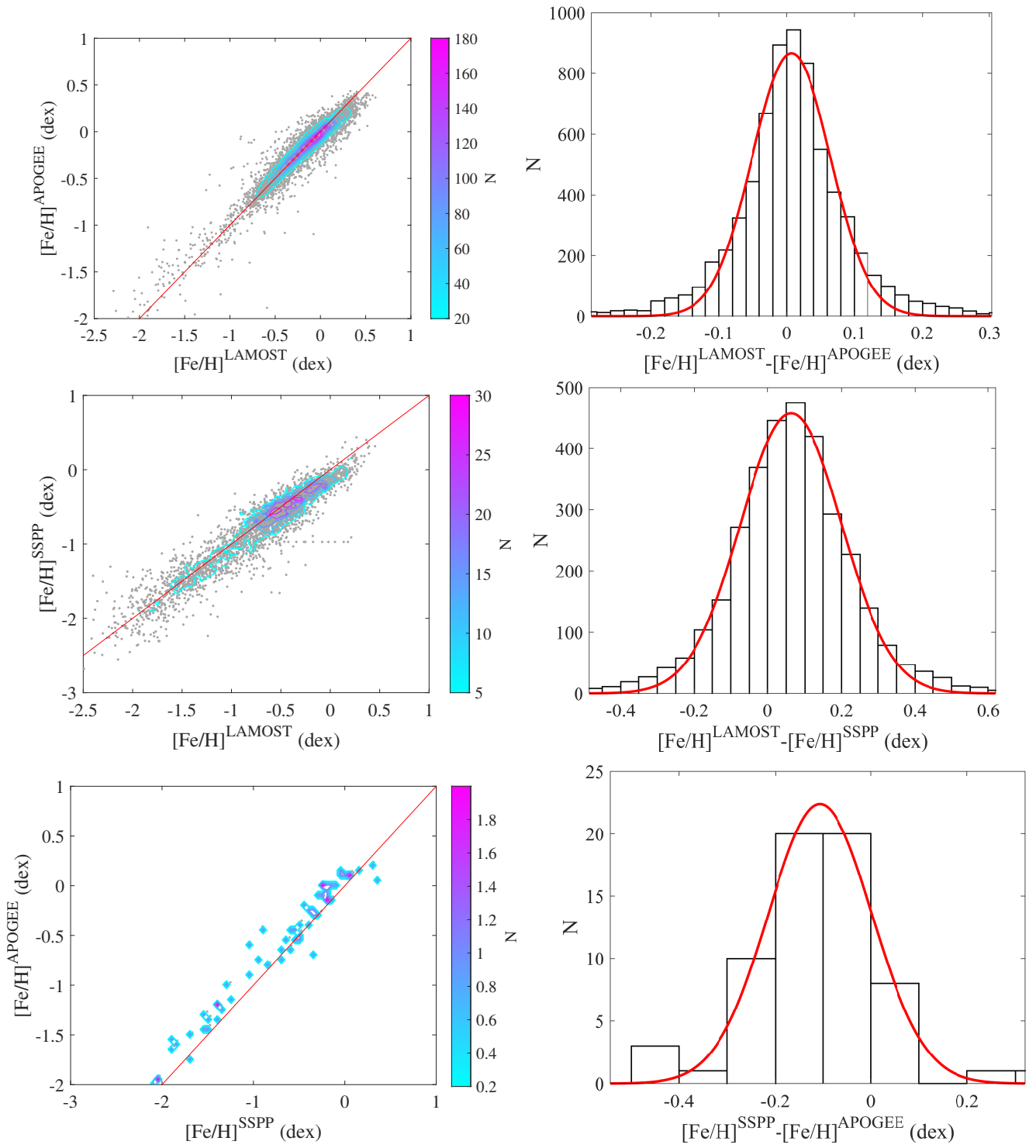


Fig. C.3. Pipeline difference of $[\text{Fe}/\text{H}]$.